
Discovering Symmetry Group Structures via Implicit Orthogonality Bias

Dongsung Huh¹

Abstract

We introduce the HyperCube network, a novel approach for autonomously discovering symmetry group structures within data. The key innovation is a unique factorization architecture coupled with a novel regularizer that instills a powerful inductive bias towards learning orthogonal representations. This leverages a fundamental theorem of representation theory that all compact/finite groups can be represented by orthogonal matrices. HyperCube efficiently learns general group operations from partially observed data, successfully recovering complete operation tables. Remarkably, the learned factors correspond directly to exact matrix representations of the underlying group. Moreover, these factors capture the group’s complete set of irreducible representations, forming the generalized Fourier basis for performing group convolutions. In extensive experiments with both group and non-group symbolic operations, HyperCube demonstrates a dramatic 100-1000 \times improvement in training speed and 2-10 \times greater sample efficiency compared to the Transformer baseline. These results suggest that our approach unlocks a new class of deep learning models capable of harnessing inherent symmetries within data, leading to significant improvements in performance and broader applicability.

1. Introduction

Deep learning has demonstrated an exceptional ability to uncover complex patterns within vast datasets. However, effectively extracting and harnessing inherent symmetries within data remains a persistent challenge. These symmetries often reflect fundamental principles and hold the key to significantly enhancing model performance, generalization, and even new scientific discoveries.

Traditional approaches often rely on manually designing specialized architectures that incorporate constraints based on known symmetries. While successful in specific domains, this strategy limits flexibility and hinders generalization to problems where symmetries are either unknown or difficult

to explicitly define.

This work introduces a paradigm shift — a novel approach that enables the automatic discovery of general group structures directly from data. Our key innovation is a unique combination of model architecture and regularizer that instills a powerful inductive bias towards learning orthogonal representations. This bias implicitly defines a complexity metric that prioritizes the discovery of general group structures. This leverages a fundamental theorem on compact/finite groups that they can be represented using orthogonal matrices. Since all compact/finite groups are intimately connected to symmetries, this eliminates the need for designing specialized architectures for specific symmetries.

To rigorously evaluate our method, we focus on the controlled yet challenging task of learning symbolic operations from incomplete data. This task provides a clear proving ground for demonstrating the ability to uncover abstract group structures.

Key Contributions:

- We reframe symbolic operation learning as a tensor completion problem, creating a fertile ground for effective solutions.
- We introduce *HyperCube* architecture and regularizer. This design decomposes the model tensor as a product of three factor tensors, while promoting the factors to learn orthogonal structures. This is key for discovering hidden group structures.
- We demonstrate that for operations with underlying group structures, HyperCube learns factors that directly correspond to the group’s orthogonal matrix representations. Remarkably, this capability extends even to certain non-group operations.
- We achieve dramatic improvements in learning various group and non-group symbolic operations. HyperCube surpasses the baseline Transformer model with a dramatic 100–1000 \times increase in learning speed and 2–10 \times greater sample efficiency.
- We show that HyperCube learns the generalized Fourier basis for performing group convolutions, establishing a fundamental link between learning symbolic

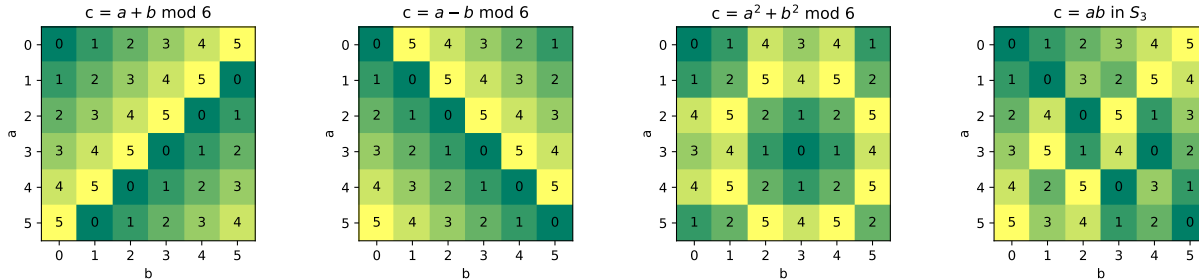


Figure 1. Small Cayley table examples: modular addition, modular subtraction, modular squared addition, and the symmetric group S_3 . Elements of S_3 are illustrated in Fig 8.

operations and acquiring the key structure needed for symmetry-aware equivariant neural networks.

2. Background

2.1. Symmetry-Constrained Architectures

Geometric Deep Learning (GDL) addresses the critical challenge of harnessing inherent symmetries within data to enhance the performance and efficiency of deep learning models (Cohen & Welling, 2016; Bronstein et al., 2021). Central to GDL is the concept of equivariance: Equivariant Neural Networks (ENNs) are designed to produce outputs that transform consistently with their inputs under a predefined group of symmetry transformations. This crucial property is achieved through group convolutions, which generalize weight-sharing in traditional CNNs to diverse symmetry groups and domains like graphs and manifolds (Kondor & Trivedi, 2018; Maron et al., 2018; Cohen et al., 2019; Bekkers, 2021).

However, explicitly encoding known symmetries into a model’s architecture has limitations. First, this approach cannot discover hidden or undiscovered symmetries prevalent in complex real-world data. Second, designing ENNs for specific groups often requires intricate architecture engineering, reducing flexibility and broader applicability. These limitations highlight the need for novel approaches that can autonomously learn symmetries directly from data. Recent efforts in this direction include (Dehmamy et al., 2021; Anselmi et al., 2019; Sanborn et al., 2023; Zhou et al., 2021).

2.2. Implicit Inductive Bias in Deep Learning

Deep learning models exhibit intrinsic preferences, known as implicit biases, that arise from their architecture and training procedures. These biases significantly influence the learning dynamics and solutions a model converges to. Implicit bias has become a focus of recent research, especially in matrix completion and deep linear networks.

In matrix completion, the goal is to recover missing entries within a data matrix, often under the assumption of low-rank

structure. Traditional approaches explicitly enforced this assumption through constraints (Burer & Monteiro, 2003) or techniques like Nuclear Norm Minimization (Fazel et al., 2001; Candès & Recht, 2009; Recht et al., 2010; Candès & Tao, 2010). In contrast, *deep matrix factorization* leverages the implicit bias of deep linear networks towards learning low-rank solutions, especially when combined with L2 regularization or small initial weights (Saxe et al., 2014; 2019). This approach demonstrates improved matrix completion performance, particularly in low-data settings (Arora et al., 2019). The low-rank bias extends beyond linear models, widely affecting the generalization behavior of nonlinear deep learning models (Jacot, 2022; Huh et al., 2023).

2.3. Symbolic Operation Completion (SOC) Tasks

Power et al. (2022) explored the potential of deep learning models for uncovering symbolic relationships within abstract operations. While conceptually similar to matrix completion, SOC involves completing tables of discrete, abstract symbols governed by binary operations (*i.e.*, Cayley tables, Figure 1). Despite successfully employing Transformer models to handle discrete symbols, Power et al. (2022) encountered significant difficulty in achieving generalization. Their models often required training times far exceeding those of simple memorization — a phenomenon termed *grokking*. Several follow-up studies further investigated this phenomenon (Liu et al., 2022; Nanda et al., 2022; Chughtai et al., 2023). This observation suggests that these models lack the ideal inductive bias to effectively solve this class of tasks.

In this work, we use SOC as a proving ground to demonstrate a powerful new framework. A key challenge in SOC lies in the absence of a well-defined *complexity metric* for symbolic operations, analogous to rank or nuclear norm in matrix completion. We address this by reformulating SOC as a tensor completion problem and introducing a novel tensor factorization approach. Our approach instills a strong bias towards learning full-rank, orthogonal representations — a fundamental shift from traditional low-rank inductive biases. Crucially, this approach implicitly defines

a complexity metric that prioritizes learning general group structures.

3. Group Representation Theory

In this section, we provide a brief introduction to groups and their representations, which defines important concepts to this work.

Groups A group (G, \circ) is a set G with a binary operation \circ that satisfies the following axioms: Closure: $\forall a, b \in G, a \circ b \in G$. Associativity: $(a \circ b) \circ c = a \circ (b \circ c)$. Identity: There exists an identity element e such that $g \circ e = e \circ g = g, \forall g \in G$. Inverse: For every element g , there exists an inverse element g^{-1} such that $g \circ g^{-1} = g^{-1} \circ g = e$.

A symmetry group is a group whose elements are functions, called transformations, and the operator is function composition.

Representations A representation of a group G on a vector space V is a *group homomorphism* $\varrho: G \rightarrow \text{GL}(V)$. This homomorphism preserves the group structure by satisfying the property:

$$\varrho(g_1 \circ g_2) = \varrho(g_1)\varrho(g_2), \quad \forall g_1, g_2 \in G. \quad (1)$$

For a real vector space of finite dimension n , we can choose a basis and identify $\text{GL}(V)$ with $\text{GL}(n, \mathbb{R})$, the group of $n \times n$ invertible real matrices.¹

Equivalent Representations Given two K vector spaces V and W , two representations $\varrho: G \rightarrow \text{GL}(V)$ and $\pi: G \rightarrow \text{GL}(W)$ are equivalent if there exists a vector space isomorphism $M: V \rightarrow W$, such that for all $g \in G$,

$$M\varrho(g)M^{-1} = \pi(g), \quad (2)$$

which is called a similarity transformation.

Unitary Representations A representation ϱ of a group G is considered *unitary* (or *orthogonal* in the case of real representation) if every matrix $\varrho(g)$ is unitary (or orthonormal) for all $g \in G$. Crucially, the *Unitarity Theorem* guarantees that any finite-dimensional representation of a compact/finite group G can be expressed as an equivalent unitary (or orthogonal) representation.

Irreducible Representations A representation is considered *reducible* if a similarity transform can decompose it into a direct sum of smaller representations. This decomposition leads to a block-diagonal matrix form, where each

block corresponds to a simpler representation. In contrast, *irreducible* representations (often abbreviated as *irreps*) cannot be broken down further. They serve as the fundamental building blocks for constructing all possible group representations.

Regular Representation Every group G possesses an inherent action on itself through translations. This internal operation can be viewed as a permutation representation, where each group element rearranges the other elements. The regular representation of G builds upon this permutation representation. It uses the permutation's basis vectors to construct a linear representation. Remarkably, the regular representation is decomposable into a direct sum of *the complete set of irreps*, where each irrep appears with a multiplicity equal to its dimension. An important property of the regular representation is that the trace of representation, also known as its *character*, is a simple function:

$$\text{Tr } \varrho(g) = \begin{cases} n, & \text{if } g = e \\ 0, & \text{otherwise.} \end{cases} \quad (3)$$

4. Notations and Definitions

We use capital symbols for order-3 tensors: e.g. T, A, B, C . T_{abc} denotes the entry of the tensor T at index (a, b, c) . T_i denotes the matrix slice of T at the first index i , and $T_{..i}$ is the slice at the third index. We employ the Einstein summation convention, where repeated indices imply summation, e.g. $A_a A_a^T \equiv \sum_a A_a A_a^T$, unless mentioned otherwise, e.g. in eq (13). We introduce the following notation for gradient $\nabla_{A_a} \mathcal{L} \equiv \partial \mathcal{L} / \partial A_a, \nabla_{T_{abc}} \mathcal{L} \equiv \partial \mathcal{L} / \partial T_{abc}$.

5. Modeling Framework

5.1. Symbolic Operations as Bilinear Maps

We model a binary operation $\mathcal{D}: S \times S \rightarrow S$ over a set S containing n distinct symbols: i.e. $\mathcal{D}(a, b) = c$, where $a, b, c \in S$. To facilitate modeling, we linearize the problem by considering a homomorphism $\phi: (S, \mathcal{D}) \rightarrow (V, \tilde{\mathcal{D}})$, where V is a vector space and $\tilde{\mathcal{D}}: V \times V \rightarrow V$ is a bilinear map. This establishes a correspondence: $\tilde{\mathcal{D}}(v^a, v^b) = v^c$, where $v^a, v^b, v^c \in V$ represent the symbols a, b, c , respectively. Specifically, we use the vector space \mathbb{R}^n with a standard basis, encoding each symbol as a one-hot vector. In this framework, the bilinear map is represented by a sparse order-3 tensor $D \in \mathbb{R}^{n \times n \times n}$, whose entries are

$$D_{abc} = \begin{cases} 1 & \text{if } \mathcal{D}(a, b) = c \\ 0 & \text{otherwise,} \end{cases} \quad (4)$$

where set elements are used as tensor indices for readability.

This framework fully expresses any binary operation \mathcal{D} on the set S as a sparse tensor D . More importantly, it

¹Our results extend to complex representations in \mathbb{C} . Here, we focus on real representations for ease of implementation within common deep learning frameworks (e.g., PyTorch, TensorFlow).

transforms the problem of learning symbolic operations from incomplete data into a tensor completion problem, where we recover the missing entries of D from the observed entries in the training set Ω_{train} .

5.2. HyperCube Factorization

To solve the tensor completion problem in Section 5.1, we approximate the desired data tensor D with a model tensor $T \in \mathbb{R}^{n \times n \times n}$. However, directly optimizing the individual entries of T as independent parameters leads to poor generalization for it treats each entry independently.

To address this, we introduce a novel parameterization, called the *HyperCube* factorization, which decomposes T into the product of three order-3 factor tensors (*i.e.*, *cubes*), $A, B, C \in \mathbb{R}^{n \times n \times n}$, all with the same dimensions as T (see Figure 2):

$$T_{abc} = \frac{1}{n} \text{Tr}[A_a B_b C_c] = \frac{1}{n} \sum_{ijk} A_{aki} B_{bij} C_{cjk}. \quad (5)$$

Crucially, this parameterization preserves the full expressive power of the model tensor T , without imposing any restrictions on its hypothesis space. This distinguishes HyperCube factorization from traditional tensor factorizations, which often employ lower-order factors (e.g., vectors or matrices) to reduce model complexity.

5.3. Regularized Loss

The model is trained by optimizing the regularized loss

$$\mathcal{L} = \mathcal{L}_o(T) + \epsilon \mathcal{H}(A, B, C) \quad (6)$$

where \mathcal{L}_o is a convex function of T , specifically the squared loss over the training set

$$\mathcal{L}_o(T) = \sum_{(a,b,c) \in \Omega_{\text{train}}} (T_{abc} - D_{abc})^2 \quad (7)$$

and \mathcal{H} is the *HyperCube* regularizer on factor pairs

$$\mathcal{H} \equiv \frac{1}{n} \text{Tr} [A_a^\top A_a B_b B_b^\top + B_b^\top B_b C_c C_c^\top + C_c^\top C_c A_a A_a^\top]. \quad (8)$$

For comparison, we also show the result of using the L2 regularizer (Figure 3, 4), *i.e.* the squared Frobenius norm:

$$\mathcal{F} \equiv \frac{1}{n} \text{Tr} [A_a^\top A_a + B_b^\top B_b + C_c^\top C_c]. \quad (9)$$

5.4. Internal Symmetry of Model

The redundant parameterization of eq (5) implies that there are multiple degrees of internal symmetry that leaves the

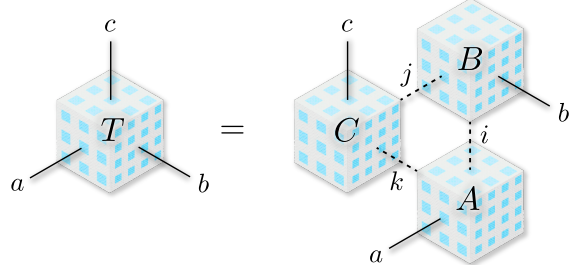


Figure 2. HyperCube factorization: The model tensor T is parameterized as a product of three order-3 factors A, B, C (see eq (5)). The internal indices (dashed lines) are contracted whereas the external indices (solid lines) are exposed as the input/output channels.

model unchanged. For example, one can introduce arbitrary invertible matrices M_I, M_J, M_K between the factors as $\tilde{A}_a = M_K^{-1} A_a M_I$, $\tilde{B}_b = M_I^{-1} B_b M_J$, and $\tilde{C}_c = M_J^{-1} C_c M_K$. These yield an equivalent parameterization of T , since the M matrices all cancel out in computing the product tensor: *i.e.* $\text{Tr}[\tilde{A}_a \tilde{B}_b \tilde{C}_c] = \text{Tr}[A_a B_b C_c]$. These symmetry transformations can be understood as changing the internal basis coordinate for representing the factors.

While $\mathcal{L}_o(T)$ is invariant under such coordinate changes, the regularizer $\mathcal{H}(A, B, C)$ is not. However, the regularizer is invariant under *orthonormal* basis changes, in which the introduced matrices are orthonormal matrices U_I, U_J, U_K , such that $U U^\top = U^\top U = I$. Therefore, the regularizer imposes a stricter form of symmetry. This leads to the following lemma.

Lemma 5.1. *If A, B, C form the optimal solution of the regularized loss eq (6), then any orthonormal basis changes leave the solution optimal, but non-orthonormal basis changes generally increase the loss.*

6. Analyzing HyperCube’s Inductive Bias

While the factorized parameterization eq (5) does not explicitly restrict the model’s hypothesis space, it exhibits a strong *implicit bias* when combined with the regularizer eq (8). In this section, we introduce key concepts that enable us to measure and analyze this inductive bias.

Definition 6.1. We define *imbalances* across edge i, j, k as

$$\begin{aligned} \xi_I &= A_a^\top (C_c^\top C_c) A_a - B_b (C_c C_c^\top) B_b^\top \\ \xi_J &= B_b^\top (A_a^\top A_a) B_b - C_c (A_a A_a^\top) C_c^\top \\ \xi_K &= C_c^\top (B_b^\top B_b) C_c - A_a (B_b B_b^\top) A_a^\top. \end{aligned}$$

Lemma 6.2. *At stationary points of the regularized loss eq (6), imbalance terms vanish to zero:*

$$\xi_I = \xi_J = \xi_K = 0. \quad (10)$$

Proof. See Appendix B for detailed proof. \square

This result generalizes the balanced condition of deep linear neural networks under L2 regularization (Arora et al., 2018; Saxe et al., 2019; Huh, 2020),

Definition 6.3 (Contracted Orthogonality). A factor A is C -orthogonal if it satisfies the following:

$$A_a A_a^\top, A_a^\top A_a \propto I \quad (11)$$

(with contraction over the repeated index a).

The following propositions demonstrate that the regularizer eq (8) promotes C-orthogonality in the factors:

Proposition 6.4. C -orthogonal factors satisfy the balanced condition eq (10), given that they share a common scalar multiple of the identity matrix:

$$\begin{aligned} A_a A_a^\top &= A_a^\top A_a = B_b B_b^\top = B_b^\top B_b \\ &= C_c C_c^\top = C_c^\top C_c = n\alpha^2 I, \end{aligned} \quad (12)$$

Lemma 6.5. Under a fixed Frobenius norm eq (9), all C -orthogonal factors are stationary points of the regularizer \mathcal{H} .

Proof. Proposition 6.4 can be confirmed in a straightforward manner. Proof for Lemma 6.5 is in Appendix C. \square

Lemma 6.5 indicates that the effect of \mathcal{H} promotes C-orthogonality while also minimizing the Frobenius norm.

Definition 6.6 (Slice Orthogonality). A factor A is S -orthogonal if every matrix slice of A is a scalar multiple of an orthonormal matrix: *i.e.*

$$A_a A_a^\top = A_a^\top A_a = \alpha_{A_a}^2 I, \quad (13)$$

(no contraction over the repeated index a).

Note that S-orthogonality is a stronger and more detailed condition than C-orthogonality. Remarkably, we make the following observation:

Observation 6.7. When optimizing the regularized loss eq (6), C -orthogonal solutions eq (12) are consistently achieved via S -orthogonality. In this case, eq (12) reduces to $\sum_a \alpha_{A_a}^2 = \sum_b \alpha_{B_b}^2 = \sum_c \alpha_{C_c}^2 = n\alpha^2$.

Although the exact mechanism driving S-orthogonality remains an open question, this surprising observation highlights the strong inductive bias towards orthogonality exhibited by the HyperCube regularizer.

7. Optimization

We employ full-batch gradient descent to optimize the regularized loss with learning rate of 0.5 and momentum of 0.5. For experiments in Section 8, the HyperCube regularizer coefficient is set to $\epsilon = 0.1$. We use $\epsilon = 0.05$ in Section 9.

ϵ -scheduler To overcome the limitations in standard regularized optimization, which often prevents full convergence to the ground truth (D), we employ ϵ -scheduler: Once the model demonstrates sufficient convergence (*e.g.* the average imbalance falls below a threshold of 10^{-5}), the scheduler sets the regularization coefficient ϵ to 0. This allows the model to fully fit the training data. The effect of ϵ -scheduler on convergence is discussed in Appendix D.

8. Small Dataset Experiments

We begin by investigating how HyperCube learns the Cayley tables in Figure 1, focusing primarily on the symmetric group S_3 . These small-scale experiments offer several advantages: they enable close examination of the model’s behavior, full visualization of its learned representations, and ultimately, a deeper understanding of the model’s key operating mechanisms.

8.1. Learning Dynamics

We analyze the model’s learning dynamics on the symmetric group S_3 as an example, with 60% of the data allocated as the training set. Figure 3 visualizes the optimization trajectories under different regularization strategies. Additionally, Figure 4 depicts the learned product tensor after training. The result of the modular addition experiment is shown in Figure 12 and 13.

Unregularized model In the absence of regularization, the model rapidly achieves perfect training loss and accuracy, but without generalizing to the unseen test dataset. The singular values remain mostly unchanged, indicating negligible structural change in the model.

\mathcal{H} regularized model With HyperCube regularization, the model steadily improves the test set performance even after the initial memorization phase. A critical turning point is observed around $t = 200$ (vertical dashed line), marked by a sudden collapse of singular values to a common value, which indicates convergence to an orthogonal solution. Indeed, from this point onward, the C-orthogonality, S-orthogonality, and imbalance measures rapidly decrease towards zero. Importantly, this internal restructuring coincides with a significant improvement in test loss and the achievement of 100% test accuracy, demonstrating its vital role in enabling generalization. Notably, when ϵ -scheduler reduces $\epsilon \rightarrow 0$ (around $t = 450$), both the train and the test losses plummet to zero, confirming perfect recovery of D .

This sudden convergence to orthogonality is also evident in Figure 9, which directly illustrates the product and factor tensors during the learning process. In stark contrast, the factors of the unregularized model remain largely unchanged from their random initial values.

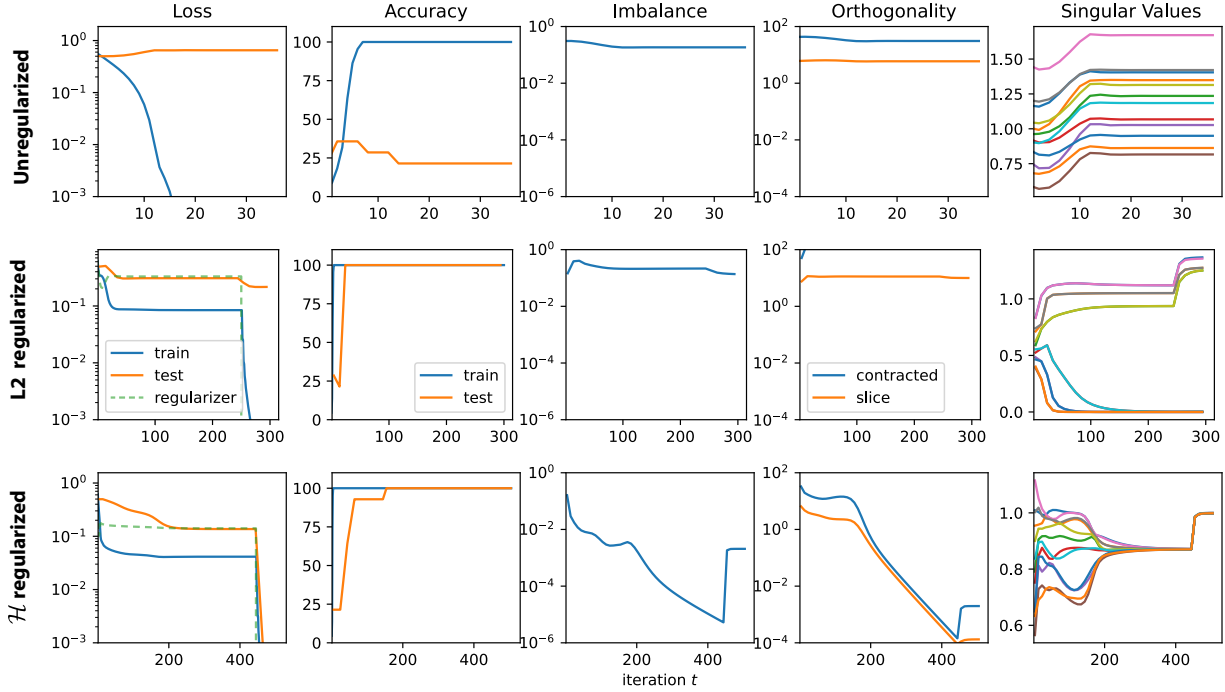


Figure 3. Optimization trajectories on the S_3 dataset with 60% of Cayley table used as the training set (See Fig 4). (Top) Unregularized, (Middle) L2-regularized, and (Bottom) \mathcal{H} -regularized training. Column 3 shows the average imbalance $(\|\xi_I\|_F^2 + \|\xi_J\|_F^2 + \|\xi_K\|_F^2)^{1/2}$, and column 4 shows deviation from C-orthogonality $\|\sum_a A_a A_a^\top / n^2 - \alpha^2 I\|_F^2$ and S-orthogonality $\|A_a A_a^\top - \alpha_{A_a}^2 I\|_F^2$, averaged over all factors and slices. Column 5 shows normalized singular values of unfolded factors A, B, C . In the \mathcal{H} -regularized case, the singular values converge to a common value, corresponding to α in eq (12). Only a subset is shown for clarity.

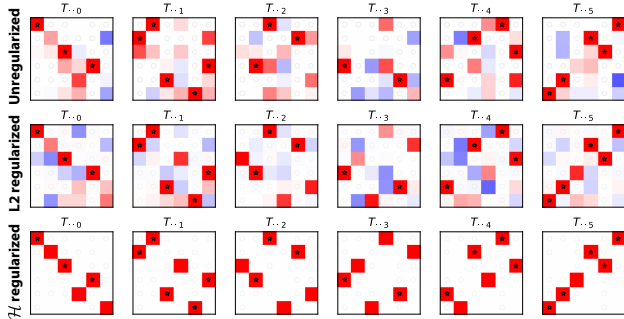


Figure 4. Visualization of product tensors after training on the S_3 dataset under different regularization strategies (see Fig 3). The observed training data are marked by asterisks (1s) and light circles (0s). (color scheme: red=1, white=0, blue=-1.) A similar visualization of the modular addition experiment is shown in Figure 13.

L2 regularized model L2 regularization drives the model towards a low-rank solution, evidenced by a portion of its singular values decaying to zero. Although the model shows some degree of generalization, it fails to reduce the test loss to zero, indicating imperfect recovery. Figure 4 visually reinforces these findings, demonstrating that both the unregularized and L2-regularized models cannot fully recover the data tensor D . Only the \mathcal{H} regularized model achieves perfect recovery. Also see Figure 12 for the modular addition

experiment result.

8.2. Learned Factors are Group Representations

This section analyzes the HyperCube factors trained on S_3 . Figure 10 visualizes the factors in different basis representations, demonstrating a remarkable finding: the learned factors directly encode group representations.

Initial Observation (top panel): In the raw coordinate representation, the factors exhibit orthogonal slices, but no other easily identifiable structure.

Key Transformation (middle panel): Applying an orthogonal basis change, such that factor slices for the identity element become the identity matrix ($A_e = B_e = C_e = I$), reveals a surprising underlying structure:

- **Weight Equality:** All factors share the same weights, meaning A_g equals B_g and also equals the transpose of C_g for any element g .
- **Group homomorphism:** The factor slices respect the underlying group structure. Multiplying slices corresponds to the group operation: *i.e.* $A_{g_1} A_{g_2} = A_{g_1 \circ g_2}$, satisfying *group homomorphism* eq (1).
- Therefore, the factor slices form a matrix representa-

tion ϱ of the group, where

$$A_g = B_g = C_g^\top = \varrho(g). \quad (14)$$

- Furthermore, the trace of factor slices satisfy eq (3), indicating that ϱ is the group’s regular representation.

Figure 11 demonstrates the group homomorphism property. The multiplication table of factor slices mirrors the structure of the group’s Cayley table (Figure 1).

Block-diagonalization (bottom panel): Representing the factors in a block-diagonalized form reveals that the regular representation ϱ indeed contains *the complete set of irreps* of S_3 . This includes the trivial (1-dim), sign (1-dim), and duplicate standard (2-dim) representations.

These findings reveal the key operating mechanism of the model: Using eq (14), the product tensor eq (5) can be expressed as

$$T_{abc} = \frac{1}{n} \text{Tr}[\varrho(a)\varrho(b)\varrho(c)^\top] = \frac{1}{n} \text{Tr}[\varrho(a \circ b \circ c^{-1})] \quad (15)$$

where the group homomorphism property is used. Using eq (3) for the trace of regular representations, it indeed follows that $T_{abc} = D_{abc}$. Note that this mechanism universally applies to all finite group operations.

The insights above lead us to the following conjecture:

Conjecture 8.1. *Let D represent a group operation table. Under the constraint $T = D$, the group representation eq (14) describes the unique minimizer of the HyperCube Regularizer eq (8), up to orthogonal basis changes.*

8.3. Discovering Structures Beyond True Groups

Figure 14 visualizes the learned factors for various small Cayley tables (modular addition, subtraction, and squared addition from Figure 1) in a block-diagonalized form. For modular addition ($a + b$), HyperCube captures the inherent cyclic group structure, and learns the regular representation $\varrho(g)$ in the factors, as described by eq (14). (See Figure 12 and 13 for more results on modular addition).

Next, we explore operations resembling groups but lacking certain axioms. Modular Subtraction ($a - b$): This operation isn’t a true group due to non-associativity. Surprisingly, HyperCube learns the same representation as addition but with transposed factors: $A_g^\top = B_g = C_g = \varrho(g)$. This intriguing behavior stems from the underlying equivalence: $a - b = c$ implies $a = c + b$, essentially *wrapping around* the group structure.

Modular Squared Addition ($a^2 + b^2$): This operation violates the inversion axiom. However, for elements with unique

inverses (e.g., $g = 0, 3$), HyperCube recovers the same representation as modular addition. For others, it learns *duplicate* representations reflecting the periodicity of squaring modulo 6: e.g., $A_2 = A_4$ and $A_1 = A_5$, since $2^2 = 4^2$ and $1^2 = 5^2$.

These diverse results highlight the remarkable power of HyperCube’s inductive bias. Even for *group-like* operations (i.e. not fully satisfying group axioms), it often generalizes and discovers meaningful, orthogonal representations. This flexibility suggests potential for broader applications beyond classic group structures.

9. Larger Dataset Experiments

Following our analysis on smaller datasets, we explore how HyperCube’s preference for orthogonal factors translates to broader generalization across diverse symbolic operations. Figure 5 presents HyperCube’s performance on datasets from Power et al. (2022), encompassing various group and non-group operations (details in Appendix A). These problems are significantly larger than our previous examples, with dimensions ranging from $n = 97$ to 120.

HyperCube demonstrates impressive generalization ability. It achieves perfect accuracy with remarkably little training data ($\sim 18\%$) on various *simple* tasks. These include group and *group-like* operations from Sec 8 with known orthogonal factor representations, as well as others lacking such representations, such as modular division (a/b), and group conjugation ($a \circ b \circ a^{-1}$ in S_5). However, for more *complex* tasks like conditional operations, $a \circ b \circ a$ in S_5 , and modular polynomials, HyperCube requires more data for effective generalization.

Interestingly, the intuitive notion of *complexity* aligns with HyperCube’s regularizer. Figure 7 shows the minimum regularizer loss \mathcal{H}^* for fitting the full operation table. Notably, group and group-like operations exhibit the lowest minimum value ($\mathcal{H}^* = 3\|D\|_F^2$), indicating their inherent simplicity to HyperCube. This metric aligns with generalization trends, where increasingly difficult tasks have higher minimum loss, culminating in the unsolvable cubic operation (modular $a^3 + ab^2 + b$). This alignment suggests \mathcal{H}^* as a reliable complexity metric.

The Transformer model from Power et al. (2022) also show a similar trend, requiring more data for complex tasks. However, it favors commutative operations (e.g., $a + b$, $a^2 + ab + b^2$) over non-commutative ones (e.g., $a - b$, $a^2 + ab + b^2 + a$, and all S_5 tasks). This may result from Transformers sharing symbol embeddings across input locations. In contrast, HyperCube handles both types equally well. Crucially, it matches or surpasses Transformer’s data efficiency on a majority of tasks, often achieving perfect accuracy with less than half the data compared to Transformer,

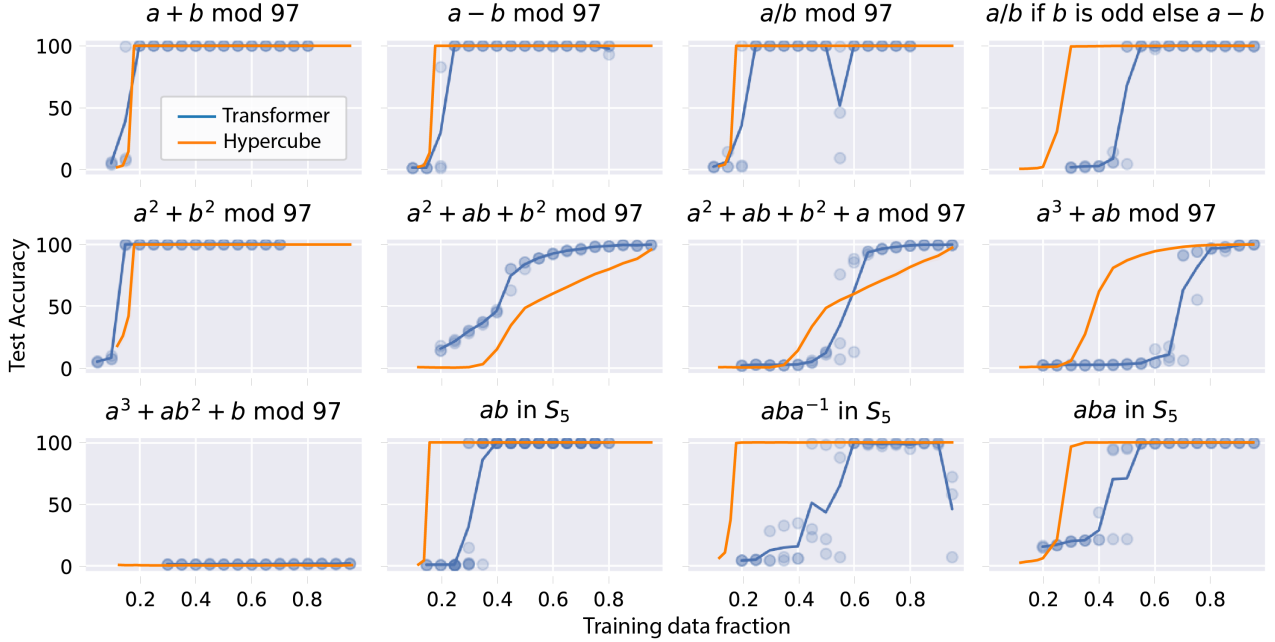


Figure 5. Comparison of average test accuracy of HyperCube (orange) vs Transformer (Power et al., 2022) (blue) on various symbolic operation tasks, as a function of training data fraction. Transformer often exhibits large variations across trials (dots), while HyperCube shows consistent performance with little trial-to-trial variations.

a remarkable 50% reduction.

Blazing-Fast Learning Beyond sample efficiency, HyperCube boasts exceptional learning speed. Figure 6 showcases its $100\times$ faster convergence to perfect accuracy compared to Transformer on the S_5 group operation, while requiring less data. Furthermore, HyperCube with shared factor weights ($A_g = B_g = C_g^T$), similar to shared embeddings in Transformers, achieves perfect accuracy with only 5% of data for training and exhibits additional $10\times$ speedup. This translates to a dramatic $1000\times$ improvement in learning speed and a 6-fold boost in sample efficiency compared to Transformer.

10. Group Convolution and Fourier Transform

Our model shares a close connection with group convolution and Fourier transform. On finite groups, the Fourier transform generalizes classical Fourier analysis to functions defined on the group: $f : G \rightarrow \mathbb{R}$. Instead of decomposing by frequency, it uses the group’s irreducible representations $\{\varrho_\xi\}$, where ξ indexes the irreps (See Appendix E.2). A function’s Fourier component at ξ is defined as:

$$\hat{f}_\xi \equiv \sum_{g \in G} f(g) \varrho_\xi(g). \quad (16)$$

10.1. Fourier Transform in HyperCube

The Fourier transform perspective offers a new way to understand how HyperCube with a group representation eq (14) processes general input vectors. Consider a vector f representing a function, *i.e.*, $f_g = f(g)$. Contracting f with a model factor A (or B) yields:

$$\hat{f} \equiv f_g A_g = \sum_{g \in G} f(g) \varrho(g), \quad (17)$$

which calculates the Fourier transform of f using the regular representation ϱ . As ϱ contains all irreps of the group, \hat{f} holds the complete set of Fourier components. Conversely, contracting \hat{f} with ϱ^T (*i.e.* factor C) performs the *inverse Fourier transform*:

$$\frac{1}{n} \text{Tr}[\hat{f} C_g] = \frac{1}{n} \sum_{g' \in G} f_{g'} \text{Tr}[\varrho(g') \varrho(g)^T] = f_g, \quad (18)$$

where eq (3) is used. This reveals that the factor tensors generalize the discrete Fourier transform (DFT) matrix, allowing the model to map signals between the group space and its Fourier (frequency) space representations.

Through the lens of Fourier transform, we can understand how the model eq (15) processes general input vectors (f and h): it calculates their Fourier transforms, multiplies them in the Fourier domain ($\hat{f}\hat{h}$), and applies the inverse Fourier transform. Remarkably, this process is equivalent to performing group convolution ($f * h$). This is because

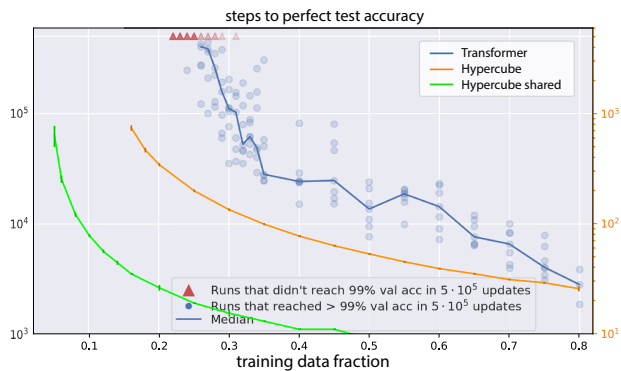


Figure 6. Comparison of training time (steps) required to achieve perfect test accuracy on the abstract group S_5 with varying amounts of training data. Models: Transformer (Power et al., 2022) (blue), HyperCube (orange), and HyperCube with shared factor weights (green, $\epsilon = 0.01$). Note the different time scales: the y-axis for HyperCube models, shown on the right, is two orders of magnitude smaller than the Transformer’s.

the linearized group operation (Section 5.1) naturally entails group convolution (see Appendix E.6,E.7).

This connection reveals a profound discovery: HyperCube’s ability to learn symbolic operations is fundamentally the same as learning the core structure of group convolutions. This means HyperCube can automatically discover the essential architecture needed for equivariant networks, without the need for hand-coded designs. This finding highlights the broad potential of HyperCube’s inductive bias, extending its applicability far beyond the realm of symbolic operations.

11. Conclusion

This work introduces HyperCube, a novel approach that enables the automatic discovery of symmetry groups from data. HyperCube implicitly defines a *complexity metric* that prioritizes learning general group structures with orthogonal internal representations.

Our findings open exciting avenues for future research. Exploring HyperCube’s inductive bias in broader domains beyond synthetic symbolic operations could uncover hidden symmetries in diverse real-world data, potentially enhancing performance and robustness of deep learning models. Additionally, we could investigate scaling the model to larger symbolic tasks such as natural language processing.

This work marks a paradigm shift in harnessing symmetries within deep learning. By enabling autonomous structural discovery and providing an intuitive measure of complexity, HyperCube has the potential to develop more flexible, generalizable, and potentially explainable deep neural networks across a wide range of applications.

References

- Anselmi, F., Evangelopoulos, G., Rosasco, L., and Poggio, T. Symmetry-adapted representation learning. *Pattern Recognition*, 86:201–208, February 2019. ISSN 0031-3203. doi: 10.1016/j.patcog.2018.07.025. URL <https://www.sciencedirect.com/science/article/pii/S0031320318302620>.
- Arora, S., Cohen, N., and Hazan, E. On the Optimization of Deep Networks: Implicit Acceleration by Overparameterization, June 2018. URL <http://arxiv.org/abs/1802.06509>. arXiv:1802.06509 [cs].
- Arora, S., Cohen, N., Hu, W., and Luo, Y. Implicit Regularization in Deep Matrix Factorization, October 2019. URL <http://arxiv.org/abs/1905.13655>. arXiv:1905.13655 [cs, stat].
- Bekkers, E. J. B-Spline CNNs on Lie Groups, March 2021. URL <http://arxiv.org/abs/1909.12057>. arXiv:1909.12057 [cs, stat].
- Bronstein, M. M., Bruna, J., Cohen, T., and Velicković, P. Geometric Deep Learning: Grids, Groups, Graphs, Geodesics, and Gauges, May 2021. URL <http://arxiv.org/abs/2104.13478>. arXiv:2104.13478 [cs, stat].
- Burer, S. and Monteiro, R. D. A nonlinear programming algorithm for solving semidefinite programs via low-rank factorization. *Mathematical Programming*, 95(2):329–357, February 2003. ISSN 1436-4646. doi: 10.1007/s10107-002-0352-8. URL <https://doi.org/10.1007/s10107-002-0352-8>.
- Candes, E. J. and Tao, T. The Power of Convex Relaxation: Near-Optimal Matrix Completion. *IEEE Transactions on Information Theory*, 56(5):2053–2080, May 2010. ISSN 0018-9448, 1557-9654. doi: 10.1109/TIT.2010.2044061. URL <http://ieeexplore.ieee.org/document/5452187/>.
- Candès, E. J. and Recht, B. Exact Matrix Completion via Convex Optimization. *Foundations of Computational Mathematics*, 9(6):717–772, December 2009. ISSN 1615-3383. doi: 10.1007/s10208-009-9045-5. URL <https://doi.org/10.1007/s10208-009-9045-5>.
- Chughtai, B., Chan, L., and Nanda, N. Neural Networks Learn Representation Theory: Reverse Engineering how Networks Perform Group Operations. In *ICLR 2023 Workshop on Physics for Machine Learning*, March 2023.
- Cohen, T. and Welling, M. Group Equivariant Convolutional Networks. In *Proceedings of The 33rd International Conference on Machine Learning*, pp. 2990–2999. PMLR, June 2016. URL <https://proceedings>.

- mlr.press/v48/cohenc16.html. ISSN: 1938-7228.
- Cohen, T., Weiler, M., Kicanaoglu, B., and Welling, M. Gauge Equivariant Convolutional Networks and the Icosahedral CNN. In *Proceedings of the 36th International Conference on Machine Learning*, pp. 1321–1330. PMLR, May 2019. URL <https://proceedings.mlr.press/v97/cohen19d.html>. ISSN: 2640-3498.
- Dehmamy, N., Walters, R., Liu, Y., Wang, D., and Yu, R. Automatic Symmetry Discovery with Lie Algebra Convolutional Network, November 2021. URL <http://arxiv.org/abs/2109.07103>. arXiv:2109.07103 [cs, math].
- Fazel, M., Hindi, H., and Boyd, S. A rank minimization heuristic with application to minimum order system approximation. In *Proceedings of the 2001 American Control Conference. (Cat. No.01CH37148)*, volume 6, pp. 4734–4739 vol.6, June 2001. doi: 10.1109/ACC.2001.945730. URL <https://ieeexplore.ieee.org/document/945730>. ISSN: 0743-1619.
- Huh, D. Curvature-corrected learning dynamics in deep neural networks. In *Proceedings of the 37th International Conference on Machine Learning*, pp. 4552–4560. PMLR, November 2020. URL <https://proceedings.mlr.press/v119/huh20a.html>. ISSN: 2640-3498.
- Huh, M., Mobahi, H., Zhang, R., Cheung, B., Agrawal, P., and Isola, P. The Low-Rank Simplicity Bias in Deep Networks, March 2023. URL <http://arxiv.org/abs/2103.10427>. arXiv:2103.10427 [cs].
- Jacot, A. Implicit Bias of Large Depth Networks: a Notion of Rank for Nonlinear Functions. September 2022. URL <https://openreview.net/forum?id=6iDHce-0B-a>.
- Kondor, R. and Trivedi, S. On the Generalization of Equivariance and Convolution in Neural Networks to the Action of Compact Groups. In *Proceedings of the 35th International Conference on Machine Learning*, pp. 2747–2755. PMLR, July 2018. URL <https://proceedings.mlr.press/v80/kondor18a.html>. ISSN: 2640-3498.
- Liu, Z., Kitouni, O., Nolte, N., Michaud, E. J., Tegmark, M., and Williams, M. Towards Understanding Grokking: An Effective Theory of Representation Learning. In *Advances in Neural Information Processing Systems*, October 2022.
- Maron, H., Ben-Hamu, H., Shamir, N., and Lipman, Y. Invariant and Equivariant Graph Networks. September 2018. URL <https://openreview.net/forum?id=Syx72jC9tm>.
- Nanda, N., Chan, L., Lieberum, T., Smith, J., and Steinhardt, J. Progress measures for grokking via mechanistic interpretability. In *The Eleventh International Conference on Learning Representations*, September 2022.
- Power, A., Burda, Y., Edwards, H., Babuschkin, I., and Misra, V. Grokking: Generalization Beyond Overfitting on Small Algorithmic Datasets, January 2022.
- Recht, B., Fazel, M., and Parrilo, P. A. Guaranteed Minimum-Rank Solutions of Linear Matrix Equations via Nuclear Norm Minimization. *SIAM Review*, 52(3):471–501, January 2010. ISSN 0036-1445, 1095-7200. doi: 10.1137/070697835. URL <http://epubs.siam.org/doi/10.1137/070697835>.
- Sanborn, S., Shewmake, C., Olshausen, B., and Hillar, C. Bispectral Neural Networks, May 2023. URL <http://arxiv.org/abs/2209.03416>. arXiv:2209.03416 [cs].
- Saxe, A. M., McClelland, J. L., and Ganguli, S. Exact solutions to the nonlinear dynamics of learning in deep linear neural networks, February 2014. URL <http://arxiv.org/abs/1312.6120>. arXiv:1312.6120 [cond-mat, q-bio, stat].
- Saxe, A. M., McClelland, J. L., and Ganguli, S. A mathematical theory of semantic development in deep neural networks. *Proceedings of the National Academy of Sciences*, 116(23):11537–11546, June 2019. doi: 10.1073/pnas.1820226116. URL <https://www.pnas.org/doi/10.1073/pnas.1820226116>. Publisher: Proceedings of the National Academy of Sciences.
- Zhou, A., Knowles, T., and Finn, C. Meta-Learning Symmetries by Reparameterization, March 2021. URL <http://arxiv.org/abs/2007.02933>. arXiv:2007.02933 [cs, stat].

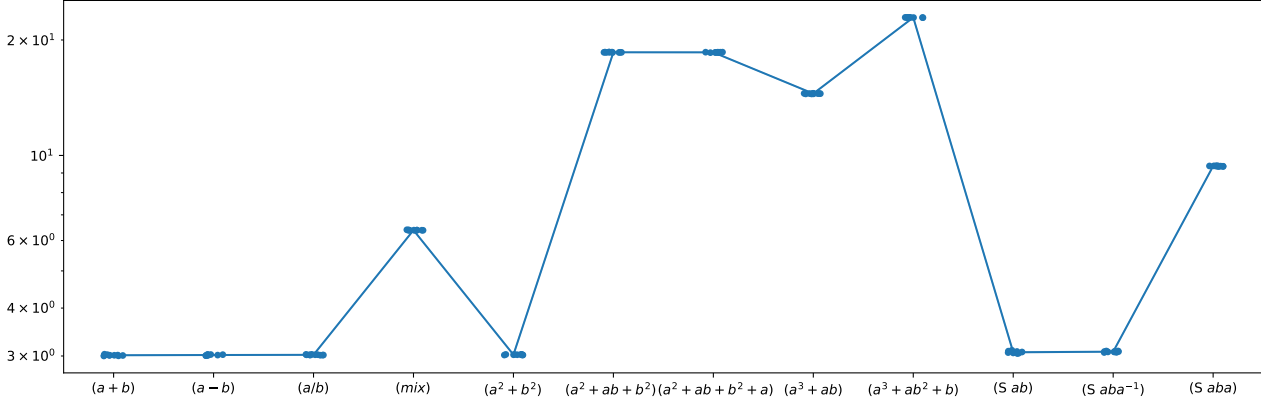


Figure 7. Minimum HyperCube regularization loss \mathcal{H} for fitting the full symbolic operation table (normalized by $\|D\|_{\mathbb{F}}^2$ to account for the size of operation). The minimum loss of $\mathcal{H} = 3\|D\|_{\mathbb{F}}^2$ is achieved by group and *group-like* operations with known orthogonal factor representations.

A. List of Binary Operations

Here is the list of binary operations from Power et al. (2022) that are used for training the model for Figure 5 and 7 (with $p = 97$ and $m = 5$).

- (add) $a \circ b = a + b \pmod{p}$ for $0 \leq a, b < p$
- (sub) $a \circ b = a - b \pmod{p}$ for $0 \leq a, b < p$
- (div) $a \circ b = a/b \pmod{p}$ for $0 \leq a < p, 0 < b < p$
- (mix) $a \circ b = [a/b \pmod{p}$ if b is odd, otherwise $a - b \pmod{p}]$ for $0 \leq a, b < p$
- (quad1) $a \circ b = a^2 + b^2 \pmod{p}$ for $0 \leq a, b < p$
- (quad2) $a \circ b = a^2 + ab + b^2 \pmod{p}$ for $0 \leq a, b < p$
- (quad3) $a \circ b = a^2 + ab + b^2 + a \pmod{p}$ for $0 \leq a, b < p$
- (cube1) $a \circ b = a^3 + ab \pmod{p}$ for $0 \leq a, b < p$
- (cube2) $a \circ b = a^3 + ab^2 + b \pmod{p}$ for $0 \leq a, b < p$
- (ab in S_m) $a \circ b = a \cdot b$ for $a, b \in S_m$
- (aba^{-1} in S_m) $a \circ b = a \cdot b \cdot a^{-1}$ for $a, b \in S_m$
- (aba in S_m) $a \circ b = a \cdot b \cdot a$ for $a, b \in S_m$

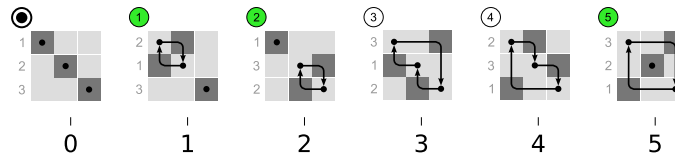


Figure 8. Elements of the symmetric group S_3 illustrated as permutations of 3 items. Green color indicates *odd* permutations, while white indicates *even* permutations. Adapted from https://en.wikipedia.org/wiki/Symmetric_group.

B. Proof of the Theorem: Balanced Condition

Here, we describe the balanced condition eq (10) in detail. First, we compute the gradient of the regularized loss $\mathcal{L} = \mathcal{L}_o(T) + \epsilon\mathcal{H}(A, B, C)$ eq (6),

$$\begin{aligned}\nabla_{A_a}\mathcal{L} &= \frac{1}{n}((\nabla_{T_{abc}}\mathcal{L}_o)C_c^\top B_b^\top + 2\epsilon(A_a(B_b B_b^\top) + (C_c^\top C_c)A_a)) \\ \nabla_{B_b}\mathcal{L} &= \frac{1}{n}((\nabla_{T_{abc}}\mathcal{L}_o)A_a^\top C_c^\top + 2\epsilon(B_b(C_c C_c^\top) + (A_a^\top A_a)B_b)) \\ \nabla_{C_c}\mathcal{L} &= \frac{1}{n}((\nabla_{T_{abc}}\mathcal{L}_o)B_b^\top A_a^\top + 2\epsilon(C_c(A_a A_a^\top) + (B_b^\top B_b)C_c))\end{aligned}\quad (19)$$

The *imbalances* in Definition 6.1 are defined as the difference of loss gradient:

$$\begin{aligned}\xi_I &\equiv \frac{n}{2\epsilon}(A_a^\top(\nabla_a\mathcal{L}) - (\nabla_b\mathcal{L})B_b^\top) = A_a^\top(C_c^\top C_c)A_a - B_b(C_c C_c^\top)B_b^\top \\ \xi_J &\equiv \frac{n}{2\epsilon}(B_b^\top(\nabla_b\mathcal{L}) - (\nabla_c\mathcal{L})C_c^\top) = B_b^\top(A_a^\top A_a)B_b - C_c(A_a A_a^\top)C_c^\top \\ \xi_K &\equiv \frac{n}{2\epsilon}(C_c^\top(\nabla_c\mathcal{L}) - (\nabla_a\mathcal{L})A_a^\top) = C_c^\top(B_b^\top B_b)C_c - A_a(B_b B_b^\top)A_a^\top\end{aligned}$$

At stationary points, *i.e.* $\nabla_a\mathcal{L} = \nabla_b\mathcal{L} = \nabla_c\mathcal{L} = 0$, imbalance terms vanish to zero, yielding the balanced condition

$$\xi_I = \xi_J = \xi_K = 0,$$

which proves Lemma 6.2.

Note that imbalance terms are defined to cancel out the $\nabla_{T_{abc}}\mathcal{L}_o$ terms. Therefore, the balanced condition is independent of the loss function \mathcal{L}_o .

C. Proof of Lemma 6.5

Proof. The constraint on Frobenius norm eq (9) can be integrated with the regularizer into an augmented loss via the Lagrange multiplier λ

$$\mathcal{H} + \lambda(\mathcal{F} - \text{constant}). \quad (20)$$

The gradient of eq (20) with respect to A_a is proportional to

$$\nabla_{A_a}(\mathcal{H} + \lambda\mathcal{F}) \propto A_a(B_b B_b^\top) + (C_c^\top C_c)A_a + \lambda A_a. \quad (21)$$

In the case of orthogonal factors B and C , all terms in eq (21) become aligned to A_a , and thus an appropriate value for the Lagrange multiplier λ can be found to vanish the gradient, which confirms stationarity. This result also applies to gradient with respect to B_b and C_c by the symmetry of parameterization. \square

D. Persistence of Group Representation

The following lemma demonstrates a key property of our model's convergence behavior: once a group representation is learned, the solution remains within this representational form throughout optimization.

Lemma D.1. *Let D represent a group operation table. Once gradient descent of the regularized loss eq (6) converges to a group representation (including scalar multiples), *i.e.**

$$A_a = \alpha_{A_a}\varrho(a), B_b = \alpha_{B_b}\varrho(b), C_c = \alpha_{C_c}\varrho(c)^\top, \quad (22)$$

the solution remains within this representation form.

Proof. With the squared loss eq (7), the gradient with respect to A_a eq (19) becomes

$$\nabla_{A_a}\mathcal{L} = \frac{1}{n}(\Delta_{abc}M_{abc}C_c^\top B_b^\top + \epsilon(A_a(B_b B_b^\top) + (C_c^\top C_c)A_a)) \quad (23)$$

where $\Delta \equiv T - D$ is the constraint error, and M is the mask indicating observed entries in the train set.

Substituting the group representation form eq (22) into eq (23), we get:

$$\frac{1}{n} \epsilon (A_a (B_b B_b^\top) + (C_c^\top C_c) A_a) = 2\epsilon \alpha_{A_a} \alpha^2 \varrho(a), \quad (24)$$

for the last two terms, where $\alpha^2 = \sum_b \alpha_{B_b}^2 / n = \sum_c \alpha_{C_c}^2 / n$.

Since the product tensor is

$$T_{abc} = \frac{1}{n} \text{Tr}[A_a B_b C_c] = \frac{1}{n} \alpha_{A_a} \alpha_{B_b} \alpha_{C_c} \text{Tr}[\varrho(a) \varrho(b) \varrho(c)^\top] = \alpha_{A_a} \alpha_{B_b} \alpha_{C_c} D_{abc},$$

and $D_{abc} = \delta_{aob,c} = \delta_{a, cob^{-1}}$ (δ is the Kronecker delta function), the first term in eq (23) becomes

$$\begin{aligned} \frac{1}{n} \sum_{b,c} \Delta_{abc} M_{abc} C_c^\top B_b^\top &= \frac{1}{n} \sum_{b,c} \delta_{aob,c} M_{abc} (\alpha_{A_a} \alpha_{B_b} \alpha_{C_c} - 1) \alpha_{B_b} \alpha_{C_c} \varrho(c \circ b^{-1}) \\ &= \frac{1}{n} \sum_b M_{ab(aob)} (\alpha_{A_a} \alpha_{B_b} \alpha_{C_{aob}} - 1) \alpha_{B_b} \alpha_{C_{aob}} \varrho(a). \end{aligned} \quad (25)$$

Note that both eq (25) and eq (24) are proportional to $\varrho(a)$. Consequently, we have $\nabla_{A_a} \mathcal{L} \propto \varrho(a)$. Similar results for other factors can also be derived: $\nabla_{B_b} \mathcal{L} \propto \varrho(b)$, and $\nabla_{C_c} \mathcal{L} \propto \varrho(c)^\top$. This implies that gradient descent preserves the form of the group representation (eq (22)), only updating the coefficients $\alpha_{A_a}, \alpha_{B_b}, \alpha_{C_c}$. \square

Effect of ϵ -Scheduler Lemma D.1 holds true even when ϵ gets modified by ϵ -scheduler, which reduces ϵ to 0. In this case, the coefficients converge to $\alpha_{A_a} = \alpha_{B_b} = \alpha_{C_c} = 1$, resulting in the exact group representation form eq (14).

E. Group Convolution and Fourier Transform

E.1. Fourier transform on groups

The Fourier transform of a function $f : G \rightarrow \mathbb{R}$ at a representation $\varrho : G \rightarrow \text{GL}(d_\varrho, \mathbb{R})$ of G is

$$\hat{f}(\varrho) = \sum_{g \in G} f(g) \varrho(g). \quad (26)$$

For each representation ϱ of G , $\hat{f}(\varrho)$ is a $d_\varrho \times d_\varrho$ matrix, where d_ϱ is the degree of ϱ .

E.2. Dual group

Let \hat{G} be a complete set indexing the irreducible representations of G up to isomorphism, called the *dual group*, thus for each ξ we have an irreducible representation $\varrho_\xi : G \rightarrow U(V_\xi)$, and every irreducible representation is isomorphic to exactly one ϱ_ξ .

E.3. Inverse Fourier transform

The inverse Fourier transform at an element g of G is given by

$$f(g) = \frac{1}{|G|} \sum_{\xi \in \hat{G}} d_{\varrho_\xi} \text{Tr} \left[\varrho_\xi(g^{-1}) \hat{f}(\varrho_\xi) \right]. \quad (27)$$

where the summation goes over the complete set of irreps in \hat{G} .

E.4. Group Convolution

The convolution of two functions over a finite group $f, g : G \rightarrow \mathbb{R}$ is defined as

$$(f * h)(c) \equiv \sum_{b \in G} f(c \circ b^{-1}) h(b) \quad (28)$$

E.5. Fourier transform of convolution

Fourier transform of a convolution at any representation ϱ of G is given by the matrix multiplication

$$\widehat{f * h}(\varrho) = \hat{f}(\varrho)\hat{h}(\varrho). \quad (29)$$

In other words, in Fourier representation, the group convolution is simply implemented by the matrix multiplication.

Proof.

$$\widehat{f * h}(\varrho) \equiv \sum_c \varrho(c) \sum_b f(c \circ b^{-1})h(b) \quad (30)$$

$$= \sum_c \varrho(c) \sum_{a,b} f(a)h(b)\delta_{(a, c \circ b^{-1})} \quad (31)$$

$$= \sum_{a,b} f(a)h(b) \sum_c \varrho(c)\delta_{(a \circ b, c)} \quad (32)$$

$$= \sum_{a,b} f(a)h(b)\varrho(a \circ b) \quad (33)$$

$$= \sum_a f(a)\varrho(a) \sum_b h(b)\varrho(b) \quad (34)$$

$$= \hat{f}(\varrho)\hat{h}(\varrho). \quad (35)$$

where δ is the Kronecker delta function, and the equivalence between $a = c \circ b^{-1}$ and $a \circ b = c$ is used between the second and the third equality. \square

E.6. Reinterpreting HyperCube's computation

HyperCube equipped with group representation eq (15) processes general input vectors f and h as

$$\begin{aligned} f_a h_b T_{abc} &= \frac{1}{n} \sum_a \sum_b f(a)h(b) \text{Tr} [\varrho(a)\varrho(b)\varrho(c)^\top] \\ &= \frac{1}{n} \text{Tr} \left[\left(\sum_a \varrho(a)f(a) \right) \left(\sum_b \varrho(b)h(b) \right) \varrho(c)^\top \right] \\ &= \frac{1}{n} \text{Tr}[(\hat{f}\hat{h})\varrho(c)^\top] = \frac{1}{n} \text{Tr}[\widehat{f * h} \varrho(c)^\top] \\ &= (f * h)_c. \end{aligned} \quad (36)$$

Therefore, the model calculates the Fourier transform of the inputs (\hat{f} and \hat{h}), multiplies them in the Fourier domain ($\hat{f}\hat{h}$), and applies the inverse Fourier transform, which is equivalent to the group convolution, as shown in Appendix E.5.

E.7. Group Convolution by D

Here we show that the linearized group operation \tilde{D} in Section 5.1 is equivalent to the group convolution in Appendix E.5.

Consider contracting the data tensor D with two functions $f, h \in G$, as

$$f_a h_b D_{abc} = \sum_{ab} f(a)h(b)\delta_{(a, c \circ b^{-1})} = \sum_b f(c \circ b^{-1})h(b) \equiv (f * h)(c), \quad (37)$$

which computes the group convolution between f and h , similar to eq (36). Here, we used $D_{abc} = \delta_{(a \circ b, c)} = \delta_{(a, c \circ b^{-1})}$.

F. Additional Figures for Section 8

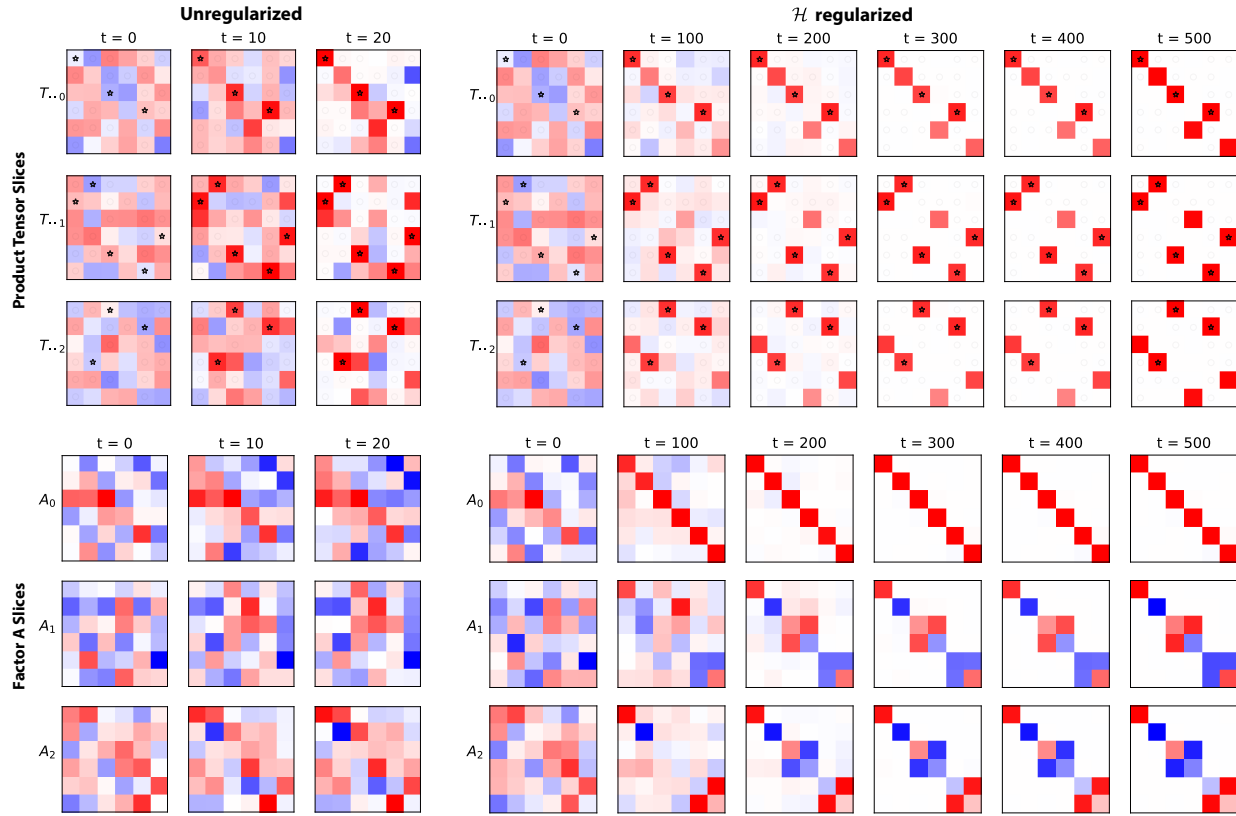


Figure 9. Visualization of product tensors during training on the symmetric group S_3 with (Right) and without (Left) regularization (see Fig 3). (Top) Product tensor slices: $T_{..c}$. The observed training data are marked by asterisks (1s) and light gray circles (0s), which are about 60% of the total data. Only the \mathcal{H} regularized model shows perfect recovery of the unmarked test data. (Bottom) Factor A slices shown in the block-diagonalizing basis coordinate of Fig 10 (Bottom). Only three slices of T and A are shown for brevity. (color scheme: red=1, white=0, blue=-1.)

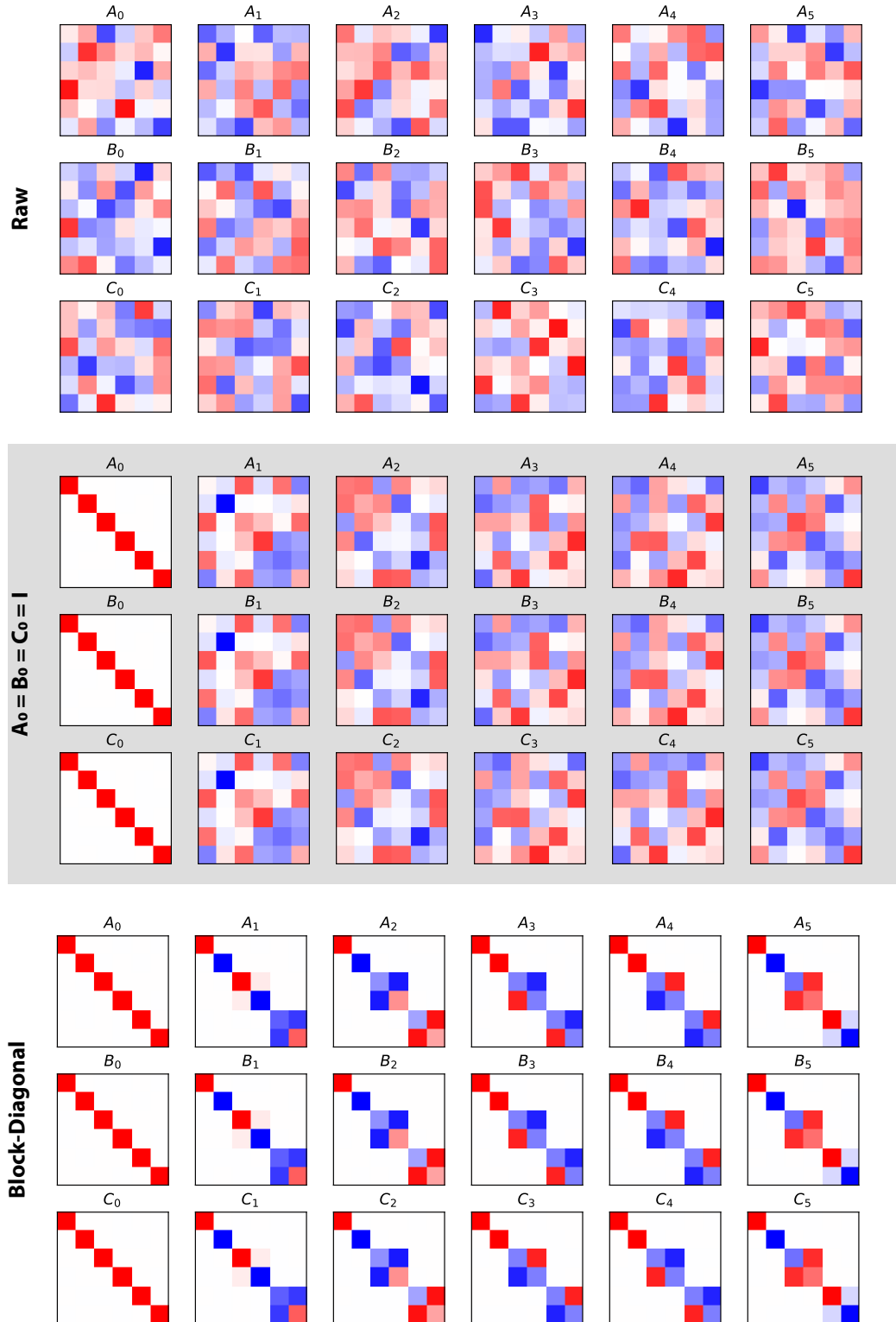


Figure 10. Learned factors of the \mathcal{H} regularized model trained on the S_3 group. (Top) Raw factor weights shown in their native coordinate representation. (Middle) Orthogonal basis change using $U_I = I, U_K = A_0, U_J = B_0^T$, which yields $\tilde{A}_0 = \tilde{B}_0 = \tilde{C}_0 = I$. (Bottom) Factors in a block-diagonalizing basis coordinate, revealing their decomposition into direct sum of irreducible representations. (color scheme: red=1, white=0, blue=-1.)

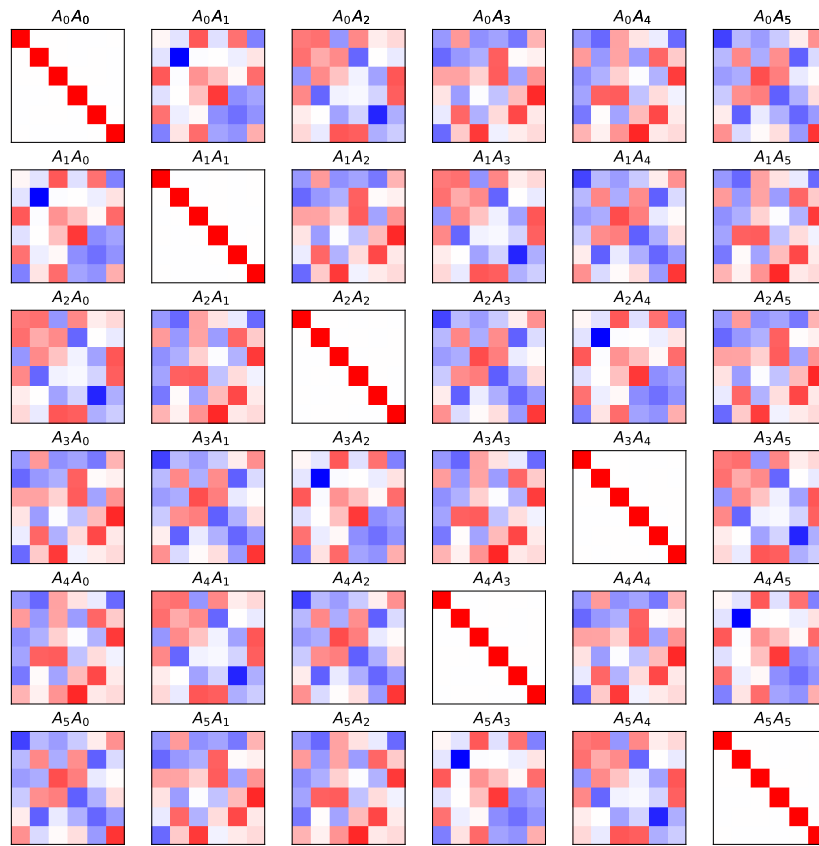


Figure 11. Multiplication table of matrix slices of factor A from the mid panel of Fig 10. Note that this table share the same structure as the Cayley table of the symmetric group S_3 in Fig 1. (color scheme: red=1, white=0, blue=-1.)

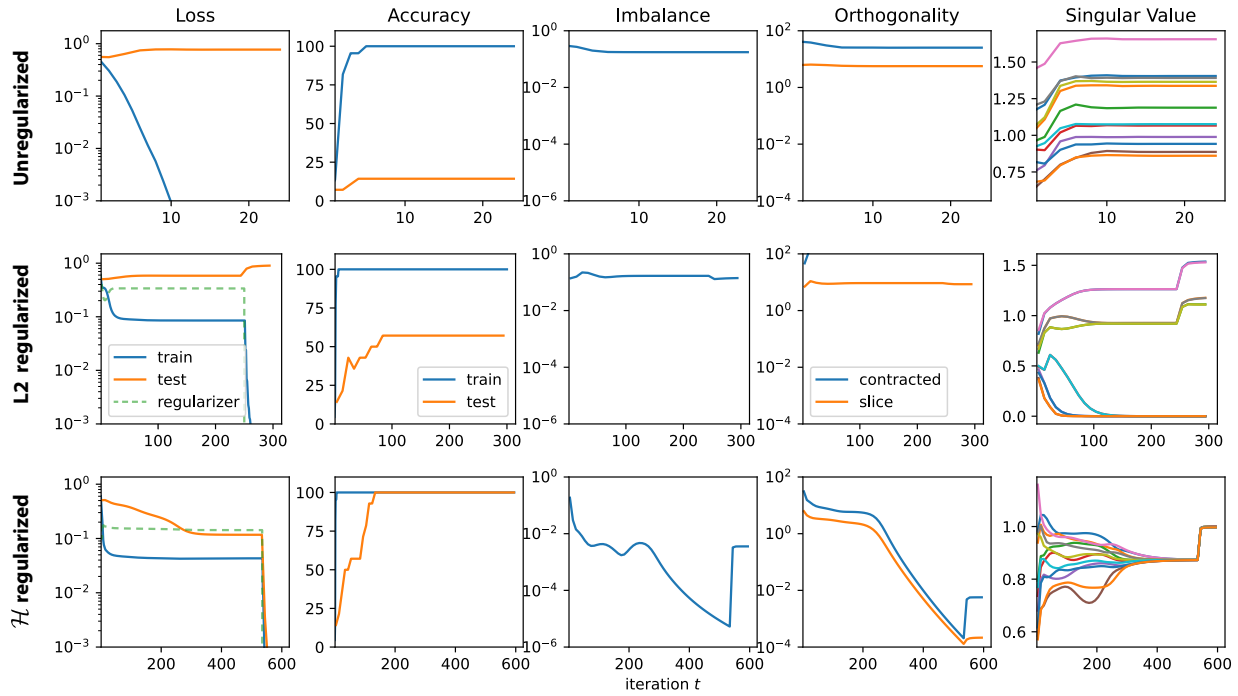


Figure 12. Optimization trajectories on the modular addition (cyclic group C_6) dataset, with 60% of the Cayley table used as train dataset (see Fig 13). (Top) Unregularized, (Middle) L2-regularized, and (Bottom) \mathcal{H} -regularized training.

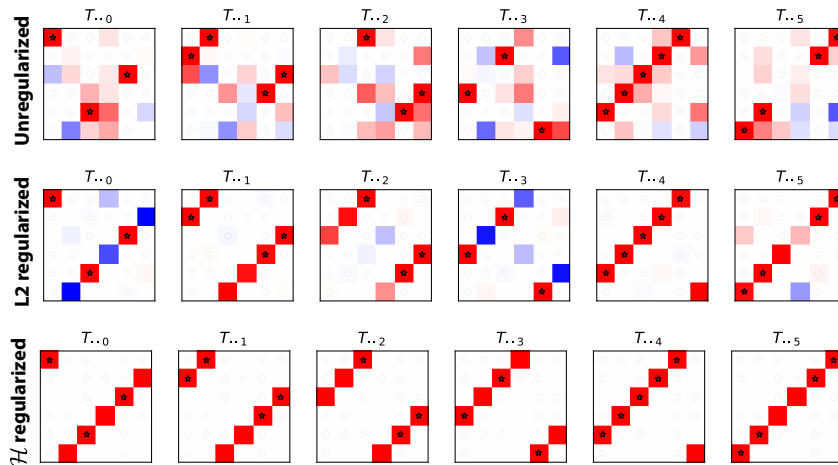


Figure 13. Visualization of product tensors after training on the modular addition (cyclic group C_6) under different regularization strategies (see Fig 12). The observed training data are marked by asterisks (1s) and gray circles (0s). Only the \mathcal{H} regularized model shows perfect recovery of the data tensor D . (color scheme: red=1, white=0, blue=-1.)

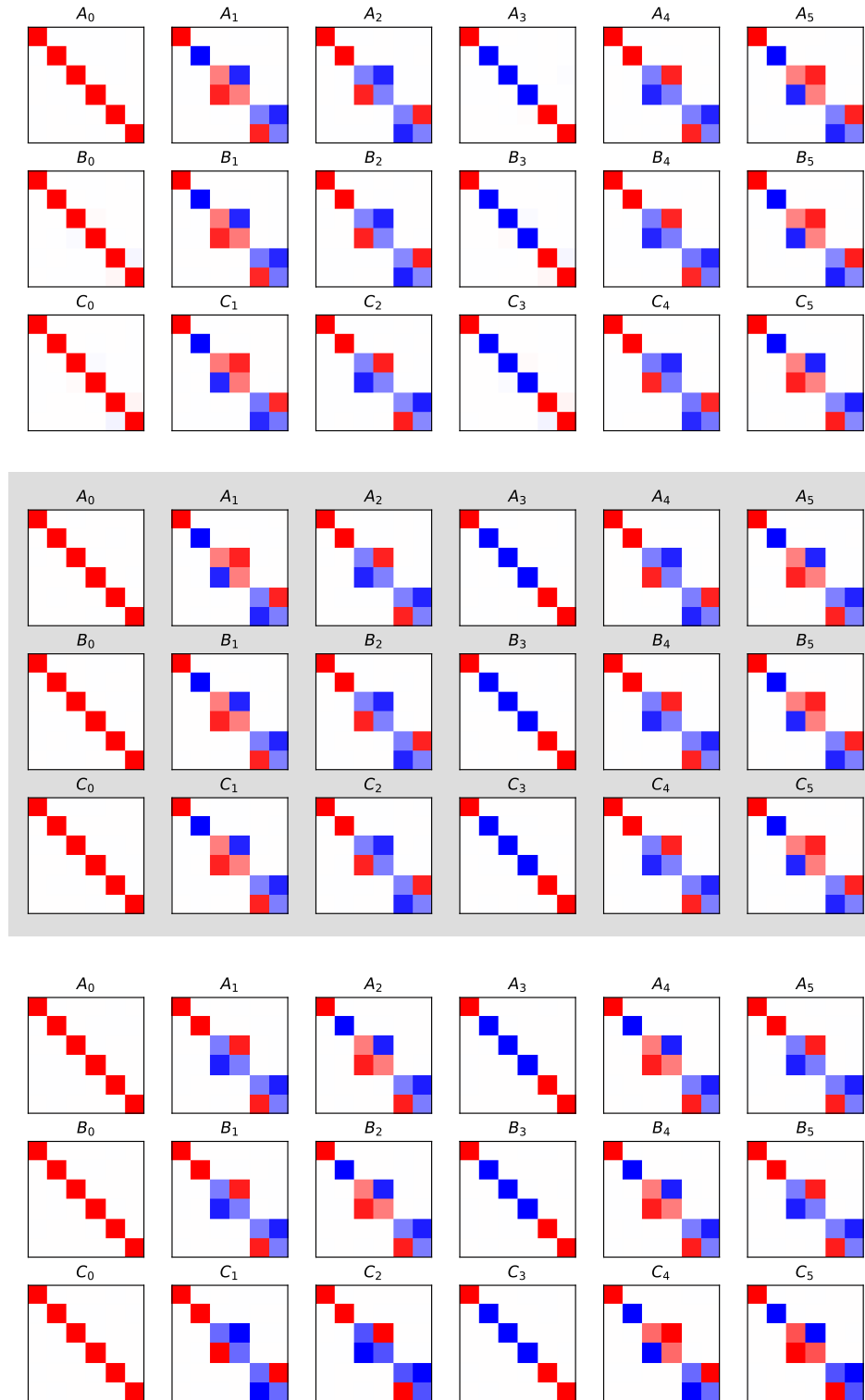


Figure 14. Visualization of factors trained on small Cayley tables from Figure 1. (Top) $c = a + b \pmod{6}$, satisfying $A_g = B_g = C_g^T = \varrho(g)$. (Middle) $c = a - b \pmod{6}$, satisfying $A_g^T = B_g = C_g = \varrho(g)$. (Bottom) $c = a^2 + b^2 \pmod{6}$, which exhibits the same representation as modular addition for elements with unique inverses (e.g., $g = 0, 3$). For others, it learns *duplicate* representations reflecting the periodicity of squaring modulo 6: e.g., $A_2 = A_4$ and $A_1 = A_5$, since $2^2 = 4^2$ and $1^2 = 5^2$. (color scheme: red=1, white=0, blue=-1.)